

# Fourier transform infrared spectroscopy-thermogravimetry analysis of the thermal decomposition mechanism of an effective flame retardant, hydroquinone bis(di-2-methylphenyl phosphate)

Lei Chen<sup>1</sup> · Zhiyi Yang<sup>1</sup> · Yan-yan Ren<sup>1</sup> ·  
Zhi-ye Zhang<sup>1</sup> · Xin-long Wang<sup>1</sup> · Xiu-shan Yang<sup>1</sup> ·  
Lin Yang<sup>1</sup> · Benhe Zhong<sup>1</sup>

Received: 17 May 2015 / Revised: 10 July 2015 / Accepted: 4 September 2015 /  
Published online: 9 September 2015  
© Springer-Verlag Berlin Heidelberg 2015

**Abstract** Hydroquinone bis(di-2-methylphenyl phosphate) (HMP) is an effective phosphorus flame retardant, but its gas flame retardant mechanism is not clear. In this study, the thermal degradation of HMP was investigated by thermogravimetry (TG) coupled with Fourier transform infrared spectroscopy (FTIR) under nitrogen and air, respectively. The results of the FTIR and semi-quantitative analyses agreed with TGA and derivative thermogravimetric analysis. Under nitrogen, the results of the TG, FTIR, and semi-quantitative analyses showed that HMP decomposed into benzyl alcohol and hydroquinone phosphate ester in a one-step process from 392 to 475 °C. Under air, the TG, FTIR, and semi-quantitative analyses showed that HMP decomposed in a two-step process. In the first step from 385 to 452 °C, HMP decomposed into benzyl alcohol, hydroquinone phosphate ester, carbon dioxide, water, and alkyne, while in the second step from 491 to 800 °C, it decomposed into carbon dioxide, water, and alkyne.

**Keywords** HMP · Flame retardant · FTIR-TG · Degradation mechanism

## Introduction

In the 1960s, halogenated flame retardants became popular due to their good flame retardant effects, low dosage, minor effects on the properties of materials, and moderate costs [1, 2]. However, the burning of polymer materials that contain halogenated flame retardants produces dioxin, as well as generating large amounts

---

✉ Lin Yang  
18980632893@163.com

<sup>1</sup> College of Chemical Engineering of Sichuan University, Chengdu, Sichuan 610065, People's Republic of China

of smoke and corrosive gases, which damage the environment and human health [3–6]. Thus, halogen-free phosphorus flame retardants that produce less smoke and toxic gases are better alternatives [7, 8], and they may also improve the overall properties of materials [9–11].

Halogen-free aryl phosphate is a form of phosphorus flame retardant, which produces less poisonous gas and it obtains good flame retardation [12]. Triphenylphosphate (TPP), resorcinol bis(diphenyl phosphate) (RDP), and bisphenol A bis(diphenyl phosphate) (BDP) are halogen-free aryl phosphate flame retardants, which are effective for use with polycarbonate/acrylonitrile–butadiene–styrene (ABS) [13, 14]. However, due to the volatility of TPP during machining process [15, 16], only RDP and BDP are commercially available [14, 17]. RDP and BDP still have many disadvantages. For example, they are liquid at room temperature, which is inconvenient for the transportation and manufacture of flame retardant products [18]. Thus, there is a tendency to use aryl phosphate flame retardants with high melting points.

Aryl phosphate flame retardants such as hydroquinone bis(diphenyl phosphate) (HDP) and hydroquinone bis(di-2-methylphenyl phosphate) (HMP) (HMP has a higher melting point than HDP), which are solid at room temperature, were synthesized in a previous study using hydroquinone, phosphorus oxychloride, and phenol for HDP, and 2-methylphenol for HMP [19, 20]. The addition of HMP and novolac phenol (NP) can increase the thermal stability of ABS at high temperatures due to the synergistic interaction between HMP and NP [20]. The composition and the flammability properties of ABS/HMP/NP composites are presented in Table 1 (when the mass ratio of HMP to NP was 2 to 1 with a total loading of 30 wt%, an LOI value of 33.5 and a UL-94 V-1 rating were obtained with a tendency toward an anti-dripping property) (Table 1). And the addition of the mixture of HMP and NP can improve the initial degradation temperature of ABS composites, which coincided with the flame retardancy properties [20]. However, the flame retardant mechanism of this composite material has not been investigated. Studying the decomposition mechanism of the flame retardant is also important for understanding the flame retardant mechanism of the composite material.

**Table 1** The composition and the flammability properties of ABS/HMP/NP composites

Sample ID	Components/(wt%)			LOI	UL-94
	ABS	HMP	NP		
ABS/HMP/NP-1	70	30	0	24.9	Failed
ABS/HMP/NP-2	70	25	5	29.7	Failed
ABS/HMP/NP-3	70	20	10	33.5	V-1
ABS/HMP/NP-4	70	15	15	29.0	Failed
ABS/HMP/NP-5	70	10	20	24.1	Failed
ABS/HMP/NP-6	70	5	25	23.1	Failed
ABS/HMP/NP-7	70	0	30	22.2	Failed
ABS	100	0	0	20.5	Failed

Many previous studies of the flame retardant action of RDP analyzed its thermal decomposition using TG, FTIR, and TG coupled with FTIR [19, 21, 22], but there have been few analyses of HDP [13, 14] and none of HMP. In the present study, we investigated the effective flame retardant HMP as the base material, where we determined its thermal decomposition to gain insights into the flame retardant mechanism. FTIR and TG were coupled to obtain the online data during the decomposition of HMP under nitrogen and air.

## Experimental

### Materials

Neat HMP was used in this study, which was synthesized using phosphorus oxychloride, hydroquinone, and 2-methylphenol in our laboratory. The HMP was purified and characterized according to a previously reported method [20].

### Measurements

FTIR-TG analysis of HMP was performed using a TGA 851 thermogravimetric analyzer, which was interfaced with a Nicolet iS10 FTIR spectrometer. A sample weighing ca 8 mg was placed in an aluminum crucible and heated from 50 to 800 °C (10 °C/min) under nitrogen and air in separate experiments (flow rate = 30 mL/min). The purge gas (nitrogen or air) pushed the pyrolysis gas products into the FTIR spectrometer throughout the thermal mass loss process via a metal pipe and glass gas pool (200 °C to avoid condensation).

## Results and discussion

### FTIR-TG analysis under nitrogen

#### *Thermogravimetric and derivative thermogravimetric analysis*

The TG and DTG curves are summarized in Table 2. Figure 1 shows the TG and DTG curves for HMP under nitrogen, which indicates that the decomposition process began at 378 °C (around that of ABS) (374 °C) [20] and ended at 475 °C.

**Table 2** Data of TG and DTG curves of HMP under nitrogen and air

Sample code	$T_{1onset}$ (°C)	$T_{1max}$ (°C)	ML I wt%	$T_{2onset}$ (°C)	$T_{2max}$ (°C)	ML II wt%	Residue wt%
HMP-N	378	426	94.6				5.4
HMP-A	385	417	80.4	491	571	14.2	4.8

*HMP-N* HMP under nitrogen, *HMP-A* HMP under air,  $T_{onset}$  initial mass loss temperature,  $T_{max}$  temperature of maximum mass loss rate, *ML* mass loss

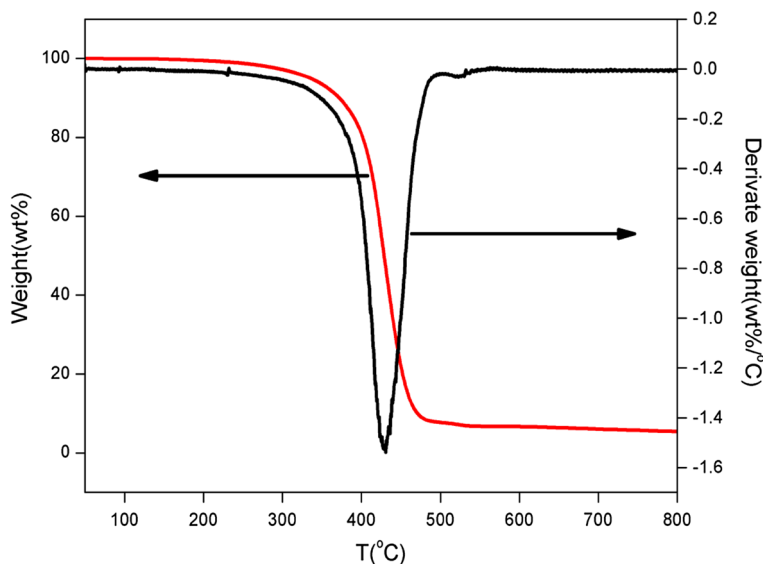


**Fig. 1** TG and DTG curves of HMP under nitrogen

The DTG curve (one peak) shows that HMP decomposed in one step under nitrogen and the temperature with the maximum mass loss rate was 426 °C (a little higher than that of ABS) (405 °C) [20]. The mass loss was 94.6 wt%/°C with a maximum mass loss rate of 1.54 wt%/°C. A char residue of 5.4 wt% was obtained, which could generate a carbon bed [20, 23] on the surface of materials to suppress burning. The mass loss corresponded to the decomposition of HMP into benzyl alcohol and phosphate ester, as demonstrated in the following FTIR analysis. The decomposition temperatures of HMP are similar to that of ABS, which means they decomposed almost together under nitrogen.

#### *FTIR analysis*

The FTIR gas phase spectra were dominated by the absorption bands of benzyl alcohol and P–O–C<sub>Ar</sub> (Fig. 2a), with C<sub>Ar</sub>–H stretching vibrations at 3073 and 3027 cm<sup>-1</sup>, and deformation vibrations of the aromatic ring of C<sub>Ar</sub>–H at 910, 772, and 695 cm<sup>-1</sup>. The –CH<sub>2</sub>– group of benzyl alcohol was also detected at 2938 and 2878 cm<sup>-1</sup>, and the –OH group at 3660 cm<sup>-1</sup>. The characteristic vibrations of the aromatic phosphate ester were also visible, with the phosphate group P–O–C<sub>Ar</sub> at 968 and 1170 cm<sup>-1</sup> (i.e., 968 cm<sup>-1</sup> for the P–O–C stretching vibration of pentavalent phosphorus and 1170 cm<sup>-1</sup> for the O–C stretching vibration). It suggests that benzyl alcohol and hydroquinone phosphate ester were produced during the degradation.

Figure 3 shows the three-dimensional (3D) FTIR spectrum for the gases produced during the thermal degradation of HMP under nitrogen. The infrared absorption peaks (around 3000 and 1000 cm<sup>-1</sup>) related to the pyrolysis products

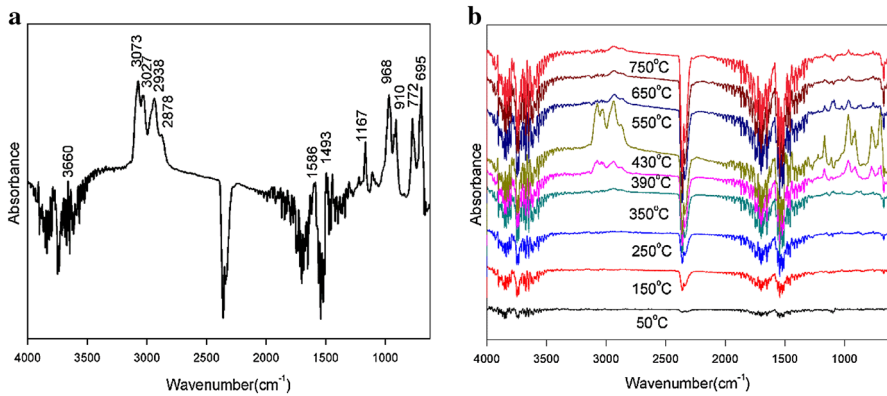


**Fig. 2** FTIR spectra of pyrolysis products for HMP at **a** 426 °C and **b** different temperatures (50, 150, 250, 350, 390, 430, 550, 650, 750 °C) under nitrogen

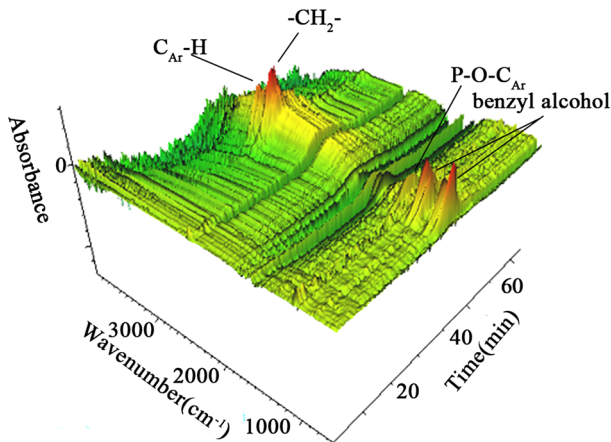


**Fig. 3** Three-dimensional diagram corresponding to gases evolved from degradation of HMP under nitrogen

(benzyl alcohol and hydroquinone phosphate ester) obtained by the thermal degradation of neat HMP began to appear after about 33 min (380 °C). The maximum intensity of the infrared absorption occurred at about 38 min (430 °C), before decreasing gradually (which corresponded to the one-step decomposition in the TG analysis). Due to the delay between TG and FTIR, the temperature was slightly higher than the  $T_{\max}$  in the TG data.

HMP decomposed in a one-step process under nitrogen according to Figs. 1 and 2. The nine FTIR spectra of the pyrolysis products were analyzed at different temperatures (50, 150, 250, 350, 390, 430, 550, 650 and 750 °C), as shown in Fig. 2b. Notable absorbance peaks were present in the spectra obtained before 390 °C. At 380 °C, small absorbance peaks indicated the beginning of pyrolysis,

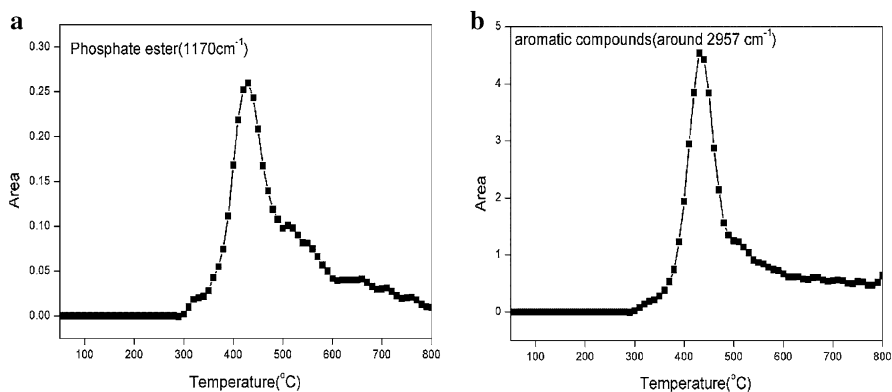
while the spectrum at 430 °C contained strong absorbance peaks, which corresponded to the temperature with the maximum mass loss rate in the TG analysis. Furthermore, there were also weak absorbance peaks in the final three spectra due to the residues of the pyrolysis products.

### Semi-quantitative analysis

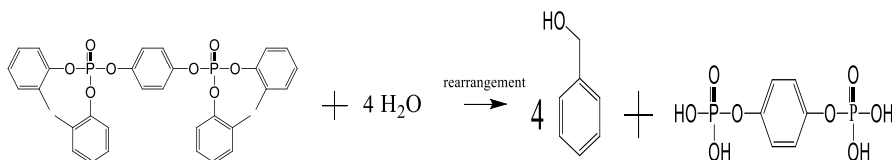
One FTIR spectrum was obtained for each 10 °C and the area of a specific wavenumber arrangement was determined using the peak area tool in the OMNIC program. The area–temperature curves were then generated. The area of each FTIR absorbance peak corresponded to the amount of each pyrolysis product released at a specific temperature.

Figure 4 shows the peak area–temperature curves obtained for the phosphate ester and aromatic compounds under nitrogen. The curves have only one peak, thereby indicating that the degradation is a one-step process. The area started to increase rapidly at about 380 °C and the peak reached its maximum at 430 °C. The temperature order of the peaks agreed with the TG and DTG analyses. However, the curves did not reach zero at 800 °C (the end of the measurement range) due to the residual gas products.

The TG-FTIR result suggests that the decomposition occurred via a one-step process where benzyl alcohol and hydroquinone phosphate ester were produced under nitrogen. The decomposition of HDP is a hydrolysis process [13]. Thus, the proposed decomposition model under nitrogen is the hydrolysis of HMP into benzyl



**Fig. 4** Release amounts of phosphate ester and aromatic compounds under nitrogen



**Fig. 5** Proposed decomposition model of HMP under nitrogen

alcohol and hydroquinone phosphate ester (Fig. 5). Rearrangements occurred during hydrolysis, which yielded benzyl alcohol. The water may come from the decomposition of HMP itself, especially for air atmosphere.

## FTIR-TG analysis under air

### TG and DTG analysis

Table 2 shows the TG and DTG data, while Fig. 6 shows the TG and DTG curves for the decomposition of HMP under air. The results suggest that HMP decomposed via a two-step process under air (Fig. 6). In the first step, decomposition started at 348 °C (lower than ABS) (374 °C) [20], which was 30 °C less than that for HMP under nitrogen, while it ended at 452 °C, which was 23 °C less than that with HMP under nitrogen. The maximum mass loss occurred at a temperature of 417 °C (a little higher than that of ABS) (405 °C) [20], which was 12 °C less than that with HMP under nitrogen. In the second step, decomposition started again at 491 °C and ended at 800 °C (the end of the TG analysis), while the temperature with the maximum mass loss rate was 571 °C. The maximum mass loss rate was 1.293 wt%/°C in the first step and 0.107 wt%/°C in the second step. The mass loss was 80.4 wt% in the first step, 14.2 wt% in the second step, and the remaining residue was 4.8 wt%. The HMP decomposition temperatures under nitrogen were slightly higher than that for HMP under air, as was the residue weight (5.4 wt% for nitrogen compared with 4.8 wt% for air). However, the decomposition rate under nitrogen (1.54 wt%/°C) was slightly faster than that under air (1.293 wt%/°C) because of the one-step decomposition process. The decomposition temperatures of HMP suggest that HMP decomposed before ABS at beginning then decomposed together, which contributed to the flame retardation of ABS.

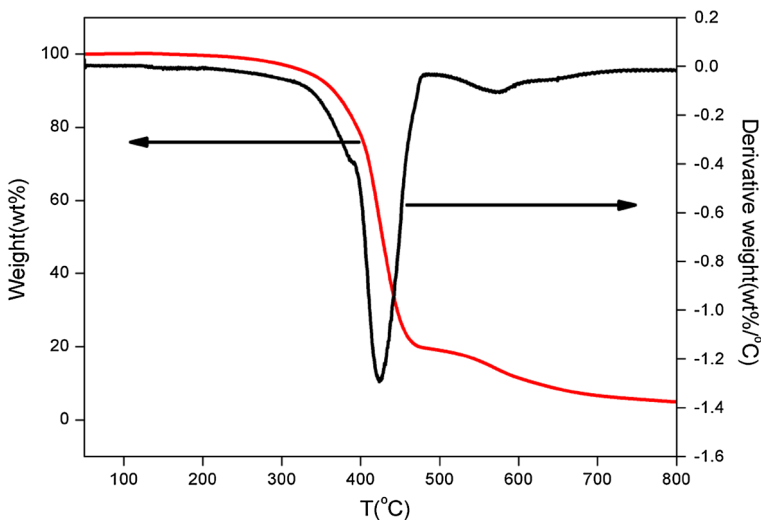


**Fig. 6** TG and DTG curves of HMP under air

### FTIR analysis

Two typical spectra (the temperatures with the maximum mass loss rates in the two steps) were selected at 420 and 570 °C (Fig. 7a, b). The large molecular products identified in Fig. 7a were similar to the products identified in Fig. 2a (benzyl alcohol and hydroquinone phosphate ester). However, some small molecular gaseous products were also released, including water (the successive peaks from 3400 to 4000  $\text{cm}^{-1}$  and from 1200 to 2100  $\text{cm}^{-1}$ ), carbon dioxide (2379, 2349, 2308 and 637  $\text{cm}^{-1}$ ), and alkyne (2182 and 2110  $\text{cm}^{-1}$ ) (Fig. 7b). The hydroquinone peaks were also clear ( $\text{C}_{\text{Ar}}\text{-H}$  stretching vibration at 3030  $\text{cm}^{-1}$ ,  $\text{C}_{\text{Ar}}\text{-H}$  deformation vibration at 771 and 745  $\text{cm}^{-1}$ , ring stretching and skeletal vibration of the aromatic ring at 1507  $\text{cm}^{-1}$ , and  $\text{-OH}$  stretching vibration at 3644  $\text{cm}^{-1}$ ).

The further combustion of the pyrolysis products (benzyl alcohol and hydroquinone) produced large amounts of  $\text{CO}_2$  and  $\text{H}_2\text{O}$ . These small molecule products can retard burning, which would be highly effective due to the large amounts of  $\text{CO}_2$  and  $\text{H}_2\text{O}$ . In addition, phosphorus oxygen free radicals ( $\text{PO}\cdot$  and  $\text{PO}_2\cdot$ ) were produced during the decomposition of phosphoric acid. The phosphorus oxygen free radicals can capture the free radicals in the air ( $\text{H}\cdot$  and  $\text{OH}\cdot$ ) and burning would be suppressed when the concentration of free radicals in the air is low [24].

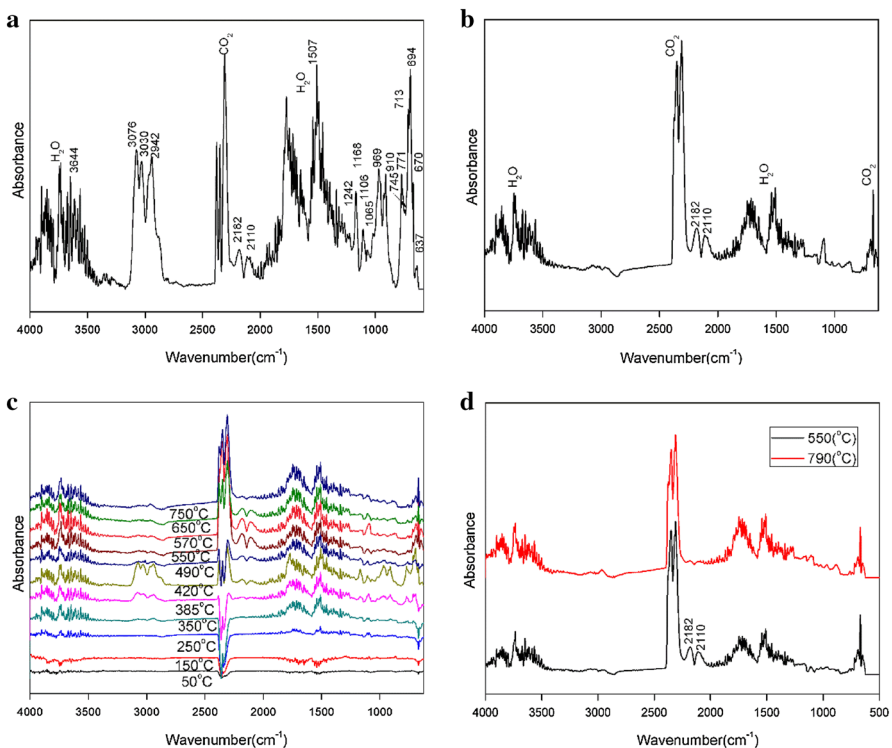


**Fig. 7** FTIR spectra of pyrolysis products for HMP under air at **a** 420 °C, **b** 570 °C, **c** different temperatures (50, 150, 250, 350, 385, 420, 490, 550, 570, 650, 750 °C) and **d** 550 and 790 °C under air



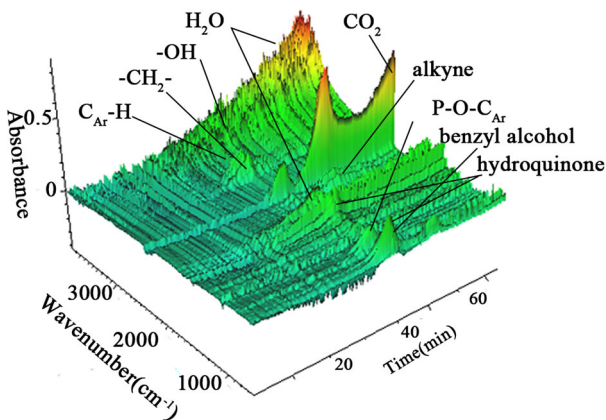
The 3D FTIR spectrum obtained under air is shown in Fig. 8. The pyrolysis products (benzyl alcohol, hydroquinone phosphate ester, water, carbon dioxide, and alkyne) started to release from about 30 min (350 °C) and they ended at about 40 min (450 °C) in the first step, while the products of further oxidization ( $\text{CO}_2$ ,  $\text{H}_2\text{O}$ , and alkyne) also started to release in the first step. The products of further oxidization continued to release from 44 min (490 °C) until 75 min (800 °C) (the end of the heating process) in the second step. This also demonstrates that the decomposition of HMP under air was a two-step process.

Thus, HMP decomposes in two steps under air according to Figs. 6 and 8. Eleven FTIR spectra of the pyrolysis products were also analyzed, which were collected at different temperatures (50, 150, 250, 350, 385, 420, 490, 550, 570, 650 and 750 °C) (Fig. 7c). The absorbance peaks of the first-step pyrolysis products (benzyl alcohol, hydroquinone phosphate ester, carbon dioxide, water, alkyne) were clear at 385 and 420 °C. The peaks were strongest at the temperature with the maximum mass loss rate (420 °C), which agreed with the TG analysis. The absorbance peaks of the products in the second step (carbon dioxide, water, and alkyne) were clear at 550, 650 and 750 °C. This result also agreed with the TG results.

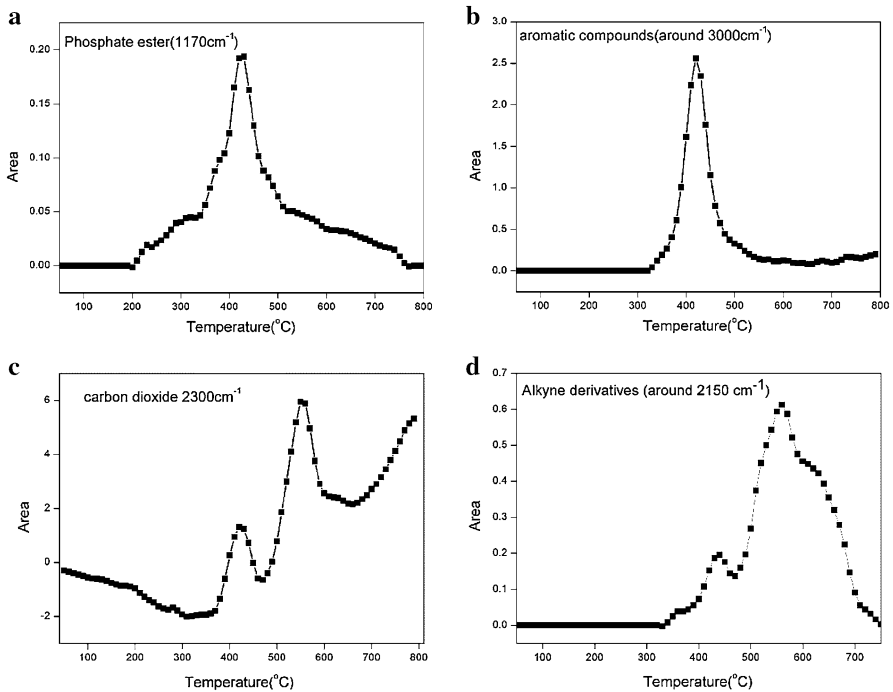
### Semi-quantitative analysis

Figure 9a, b shows the area–temperature curves for phosphate ester and aromatic compounds under air. Both curves have one peak, which suggests that the generation of the two products is a one-step process. The temperature of the peak was 420 °C, which was similar to the  $T_{1\text{max}}$  of the TG curve. The areas of the pyrolysis products were slightly larger under nitrogen compared with air. This was mainly due to the further pyrolysis under air, which directly reduced the amount of pyrolysis products during the first step.

Carbon dioxide was produced under air. There were three pyrolysis steps for carbon dioxide (the first two steps corresponded to the two pyrolysis steps for HMP



**Fig. 8** Three-dimensional diagram corresponding to gases evolved from degradation of neat HMP in the temperature interval 50–800 °C under air



**Fig. 9** Release amounts of **a** phosphate ester, **b** aromatic compounds, **c** carbon dioxide and **d** alkyne under air

under air, but the third step was not clear in the TG and DTG curves) (Fig. 9c). The two temperatures of the first two peaks occurred at 420 and 570 °C, which were similar to  $T_{1\max}$  and  $T_{2\max}$  in the TG analysis. After the second peak, the area increased with the temperature until the end of the heating process, which comprised the third step.

However, the third step was not clear for carbon dioxide in the TG and DTG curves, it should be related to the temperature almost at the end of pyrolysis. The results shown in Fig. 7d demonstrate that alkyne was not produced in the third step (no peaks at 2182 and 2110  $\text{cm}^{-1}$  in the FTIR spectrum at 790 °C). Low amount of small molecules (carbon dioxide and water) was not present in the TG and DTG curves. Figure 9d shows the area–temperature curve for alkyne derivatives, where the two peaks correspond to the two-step pyrolysis process. The second peak is higher than the first peak, which also shows that the second-step mass loss in the TG curve was related mostly to the release of alkyne.

Thus, it was inferred from the discussion above that the first step corresponds mainly to the decomposition of HMP into benzyl alcohol and hydroquinone phosphate ester (Fig. 10a), whereas the second step corresponds mainly to the further oxidization into alkyne, carbon dioxide, and water (Fig. 10b). According to a previous study [24], we infer that the phosphoric acid decomposed into phosphorus oxygen free radicals ( $\text{PO}\cdot$  and  $\text{PO}_2\cdot$ ), which would capture the free radicals in the air

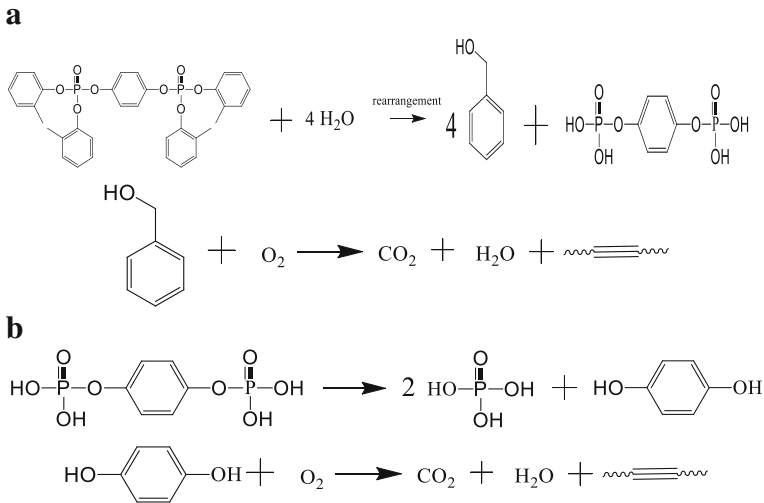


**Fig. 10** Proposed **a** first-step and **b** second-step decomposition model of HMP under air

**Table 3** Proposed flame retardation mechanism of pyrolysis products under air

Components	Mass loss step	Retardation method
Benzyl alcohol	Mass loss 1	Dehydration charring
Hydroquinone phosphate ester	Mass loss 1	Produce $\text{PO}\cdot$ and $\text{PO}_2\cdot$ to capture $\text{H}\cdot$ and $\text{OH}\cdot$ in the air
Carbon dioxide	Mass loss 1 and 2	Dilute the oxygen content in the air
Water	Mass loss 1 and 2	Absorb heat and produce water vapor to dilute the oxygen content
Alkyne	Mass loss 1 and 2	
Phosphorus acid	Mass loss 2	Produce $\text{PO}\cdot$ and $\text{PO}_2\cdot$ to capture $\text{H}\cdot$ and $\text{OH}\cdot$
Hydroquinone	Mass loss 2	Dehydration charring

( $\text{H}\cdot$  and  $\text{OH}\cdot$ ), thereby suppressing the fire. Proposed flame retardation mechanism of pyrolysis products under air is presented in Table 3.

## Conclusion

In this study, we investigated the thermal degradation behavior of HMP under nitrogen and air based on FTIR and TG analyses. The thermal degradation processes differed under nitrogen and air. Under nitrogen, the TG and DTG analysis suggests that HMP decomposed via a one-step process. The FTIR analysis indicates that HMP decomposed mostly into benzyl alcohol and hydroquinone phosphate ester.

The semi-quantitative analysis also shows that the release of aromatic compounds and phosphate ester is a one-step process. Under air, the TG and DTG results indicate that HMP decomposed via a two-step process. The FTIR analysis demonstrates that HMP decomposed into benzyl alcohol, hydroquinone phosphate ester, carbon dioxide, water, and alkyne derivatives in the first step, whereas the second step corresponds mainly to further oxidization into carbon dioxide, water, and alkyne. The semi-quantitative analysis shows that the aromatic compounds and phosphate ester are released via a one-step process. Carbon dioxide was released in a third step and alkyne was released in a two-step process. The results of the FTIR and semi-quantitative analyses agree with the TG analysis. Thus, the flame retardant effect relies mainly on the release of carbon dioxide and water, the pyrolysis of phosphoric acid, and the formation of a carbon bed. Carbon dioxide can suppress the flames and water can absorb heat. The pyrolysis products of phosphoric acid (phosphorus oxygen free radicals) may also play important roles in flame retardation by combining with free radicals in the air. And the carbon bed forms a layer that protects materials from burning.

**Acknowledgments** This paper is based on the results from the subject supported by National High Technology Research and Development Program of China (Grant No. 2011AA06A106) and Young Teachers Scientific Research Foundation Project of Sichuan University (2012SCU11024).

## References

1. Chen HR, Li XD (2012) The recent progress of flame retardants. *Fiber Compos* 1:18–21
2. Tang RG, Huang ZG (2012) Perspectives of halogenated flame retardant. *Bull Sci Technol* 28:128–132
3. Kim JS, Klösener J et al (2014) Toxicity assessment of air-delivered particle-bound polybrominated diphenyl ethers. *Toxicology* 317:31–39
4. Garcia-Reyero N, Escalon BL, Prats E et al (2014) Effects of BDE-209 contaminated sediments on zebrafish development and potential implications to human health. *Environ Int* 63:216–223
5. Colnot T, Kacew S, Dekant W (2014) Mammalian toxicology and human exposures to the flame retardant 2,2',6,6'-tetrabromo-4,4'-isopropylidenediphenol (TBBPA): implications for risk assessment. *Arch Toxicol* 88:553–573
6. Lu SY, Hamerton I (2002) Recent developments in the chemistry of halogen-free flame retardant polymers. *Prog Polym Sci* 27:1661–1712
7. Schartel B (2010) Phosphorus-based flame retardancy mechanisms—old hat or a starting point for future development? *Materials* 3:4710–4745
8. Lv Q, Huang JQ, Chen MJ et al (2013) An effective flame retardant and smoke suppression oligomer for epoxy resin. *Ind Eng Chem Res* 52:9397–9404
9. Wang DY, Ge XG, Wang YZ et al (2006) A novel phosphorus-containing poly (ethylene terephthalate) nanocomposite with both flame retardancy and anti-dripping effects. *Macromol Mater Eng* 291:638–645
10. Ye JH, Liang GZ, Gu AJ et al (2013) Novel phosphorus-containing hyperbranched polysiloxane and its high performance flame retardant cyanate ester resins. *Polym Degrad Stab* 98:297–305
11. Liao FH, Zhou L, Ju YQ et al (2014) Synthesis of a novel phosphorus-nitrogen-silicon polymeric flame retardant and its application in poly(lactic acid). *Ind Eng Chem Res* 53:10015–10023
12. Jiang Z, Zhao J (2012) Flame retardancy, smoke suppression effect and mechanism of aryl phosphates in combination with magnesium hydroxide in polyamide 6. *J Wuhan Univ Technol Mater Sci Ed* 27:916–923
13. Despinasse MC, Schartel B (2012) Influence of the structure of aryl phosphates on the flame retardancy of polycarbonate/acrylonitrile–butadiene–styrene. *Polym Degrad Stab* 97:2571–2580

14. Despinasse MC, Schartel B (2013) Aryl phosphate–aryl phosphate synergy in flame-retarded-bisphenol A polycarbonate/acrylonitrile-butadiene-styrene. *Thermochimica Acta* 563:51–61
15. Green J (2000) Phosphorus-containing flame retardants. Fire retardancy of polymeric materials, pp 147–170
16. Yoon D, Jung HT, Kwon G et al (2013) Dynamics and mechanism of flame retardants in polymer matrixes: experiment and simulation. *J Phys Chem B* 117:8571–8578
17. Ballesteros-Gomez A, Eede NV, Covaci A (2015) In vitro human metabolism of the flame retardant resorcinol bis(diphenylphosphate)(RDP). *Environ Sci Technol* 49:3897–3904
18. Nguyen C, Kim J (2008) Thermal stabilities and flame retardancies of nitrogen–phosphorus flame retardants based on bisphosphoramidates. *Polym Degrad Stab* 93:1037–1043
19. Fu QJ, Wang XL, Zhang ZY et al (2013) Synthesis and application of phosphorus flame retardant HDP ABS composites. *Acta Polymerica Sin* 2:166–173
20. Ren YY, Chen L, Zhang ZY et al (2014) Synergistic effect of hydroquinone bis(di-2-methylphenyl phosphate) and novolac phenol in ABS composites. *Polym Degrad Stab* 109:285–292
21. Bright DA, Dashevsky S, Moy PY et al (1997) Resorcinol bis (diphenyl phosphate), a non-halogen flame-retardant additive. *J Vinyl Add Tech* 3:170–174
22. Murashko EA, Levchik GF, Levchik SV et al (1999) Fire-retardant action of resorcinol bis (diphenyl phosphate) in PC–ABS blend. II. Reactions in the condensed phase. *J Appl Polym Sci* 71:1863–1872
23. Enescu D, Frache A, Lavaselli M et al (2013) Novel phosphorus-nitrogen intumescent flame retardant system. Its effects on flame retardancy and thermal properties of polypropylene. *Polym Degrad Stab* 98:297–305
24. Lu LN, Ou ZH (2008) Research progress of halogen-free flame retardant PC/ABS alloy, China. *Elastomers* 25:168–170